Journal of Materials Chemistry A

Accepted Manuscript

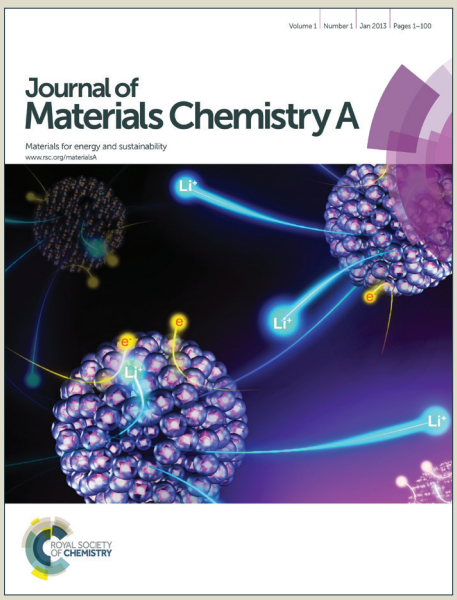

ROYAL SOCIETY OF CHEMISTRY

www.rsc.org/materialsA

Journal of Materials Chemistry A

Journal of Materials Chemistry A

RSC Publishing ▶

Cite this: DOI: 10.1039/c0xx00000x

PAPER

www.rsc.org/xxxxxx

Solvent evaporation plus hydrogen reduction method to synthesize IrNi/C catalysts for hydrogen oxidation

Weiwei Zhang, Wei Ding, Siguo Chen, Li Li, Hongmin Wang and Zidong Wei *

Received (in XXX, XXX) Xth XXXXXXXXX 20XX, Accepted Xth XXXXXXXXX 20XX

DOI: 10.1039/b000000x

A solvent evaporation plus hydrogen reduction (SE-HR) method is developed for the synthesis of carbon supported IrNi nanoparticles (IrNi/C) by using ammonia as a complexing agent. In this method, well distributed $Ni(NH_3)_nIrCl_6$ complexes are formed and adsorbed on the carbon support; after thermal annealing, high dispersed IrNi nanoparticles are obtained by in situ reduction of the corresponding complexes. By varying preparation conditions, IrNi/C samples with the lattice parameter of Ir controlled in the range from 3.8416 Å to 3.6649 Å are prepared. The hydrogen oxidation reaction (HOR) of the IrNi/C exhibits volcano-shaped dependence on the lattice parameter of Ir with a maximum activity at 3.7325 Å. The mass activity of the as-synthesized catalysts is higher than or comparable to that of commercial Pt/C catalysts in three-electrode test and single cell test. The high activity is ascribed to the optimal interaction between the catalyst surface and the hydrogen intermediates, and to the high specific electrochemical activity surface area resulted from the novel SE-HR method.

Introduction

The proton exchange membrane fuel cells (PEMFCs) are promising power sources due to their high energy efficiency and environmental compatibility; while a critical barrier in dissemination of PEMFCs is the extreme dependence on platinum as both anode and cathode electrocatalysts.[1-3] Much effort has been put into the commercialization of PEMFCs in recent years.[4-6] There are several promising alternative materials reported recently as cathode catalysts for oxygen reduction.[7-10] On the anode side for hydrogen oxidation reaction, however, the research has focused on reducing the amount of Pt[11] and a few studies on non-Pt anode electrocatalysts have reported disappointing performance so far.[12] Because the electrocatalysts account for the highest cost factor for PEMFC stack, it is urgently needed to find new, high-efficiency and low-cost non-Pt anode electrocatalysts.

In recent years, Ir has attracted considerable attention as one of the promising Pt-alternative anode catalysts due to its cheaper price and acceptable activity in acidic media.[13, 14] It has been found that upon appropriate modification of their surface atomic structure, Ir-based nanomaterials can become promising electrocatalysts by simultaneously decreasing the material cost and enhancing the performance. [15-18] Therefore, controlling the morphology of these Ir-based nanocrystals has great signification on the practical application because the catalytic activity and stability are strongly correlated with the shape and size of the nanocrystals. Besides fuel cell catalysts, size control of metal nanoparticles (NPs) produces unique catalytic properties, and well designed nanosized non-Pt metal catalysts sometimes show higher performance than a Pt catalyst.[19, 20] Several facile methods have been developed to rapidly synthesize non-Pt catalysts with predefined composition, structure, and catalytic properties. [10, 21, 22] These beneficial and attractive effects of structural control inspired us to develop a non-Pt anode catalyst having higher or comparable catalytic activity to Pt by fine-tuning of the catalyst structure in nanoscale. Generally, the synthesis of Ir-based bimetallic NPs is relied on a successive solution-phase chemical reduction plus H_2 annealing method. To get NPs with controlled particle size and composition, the special reducing agent, surfactants and organic solvents are usually thought essential; harsh conditions are also required in the synthesis of the alloys. There are two fundamental issues in terms of the conventional method: (1) the particles may suffer inevitable second growth of particle size during the thermal annealing; (2) surface residues from reducing agent and organic solvent would deactivate the catalysts. [23]

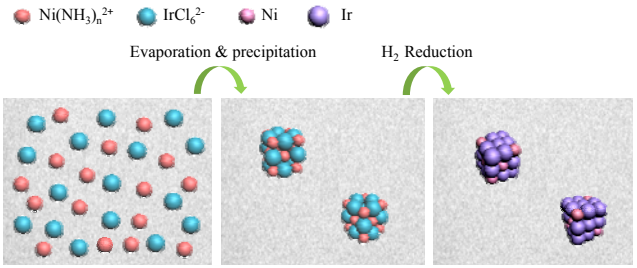

Fig. 1 Scheme for the synthesis of IrNi/C by using the SE-HR method.

Herein, we report a novel and straightforward solvent evaporation plus hydrogen reduction (SE-HR) method for the synthesis of high-HOR-activity IrNi/C catalysts by using ammonia as both a complexing agent and pH regulator. The synthesis strategy is shown in Fig. 1. The ammonia was added to the suspension of metal precursors and leaded Ni to form $Ni(NH_3)_n^{2+}$ complex cations, while Ir was still in complex anions presented as $IrCl_6^{2-}$. Being different from conventional chemical reduction method, the suspension was directly evaporated to dryness in water bath and subsequently reduced in H_2 atmosphere. In the solvent evaporation process, the Ir and Ni complexes spontaneously attracted each other by electrostatic attraction to get well distributed $Ni(NH_3)_nIrCl_6$ precipitation. Thus, well dispersed IrNi composite NPs with an average size of sub-3 nm were obtained by in situ reduction and nucleation of Ir, Ni in H_2 atmosphere. The slow-release of the Ir, Ni atoms from the $Ni(NH_3)_nIrCl_6$ complexes during the annealing contributes to the small size and uniform distribution of the alloy NPs. To optimize the catalytic activity, the synthesis conditions of IrNi/C catalysts were investigated systematically with regard to pH regulator, annealing temperature and molar ratio of metal precursors. Electrochemical measurements confirmed that IrNi/C shows the excellent HOR performance in PEMFCs. Interestingly, a unique lattice parameter dependent HOR activity of the catalysts was first found when plotting the measured mass activity to the lattice parameter of Ir.

Experimental

Catalyst synthesis

In a typical synthesis of IrNi/C NPs, $H_2IrCl_6•6H_2O$ and $NiCl_2•6H_2O$ were chosen as Ir and Ni precursors, respectively. At first, a well-distributed suspension of carbon black (Vulcan XC-72R) in deionized water was formed by ultrasonicating and stirring over 30 min. Then metal precursors with different initial Ir/Ni molar ratios were added into the suspension for a total metal loading of 20 wt%. Meanwhile, appropriate amount of sodium citrate (TCD) was added as a protective agent. After ultrasonicating and stirring constantly for overnight, appropriate amount of $NH_3•H_2O$ or NaOH solution was added into the suspension to reach a pH of 12. Note that IrNi/C sample without adjusting pH was also prepared for comparison. Then, the mixture was stirred for overnight in a sealed state and then evaporated to dryness at 60 ˚C in a water bath. The obtained precipitations were heat-treated at 300, 400, 500 and 600 ˚C respectively in a tube furnace under the mixture gas flow of N_2 and H_2 (6:1) for 2 h and then cooled down to room temperature. The resultant black powders were filtered, washed with deionized water, and dried at 60 ˚C for 6 h.

The samples (Ir/Ni=1/1, annealed at 500 ˚C) adjusted pH with $NH_3•H_2O$ or NaOH aqueous solution are denoted as IrNi/C-NH_3-500, IrNi/C-NaOH-500, respectively. The sample obtained without adjusting pH is denoted as IrNi/C-500. Similarly, the samples (adjusted pH with $NH_3•H_2O$, annealed at 500 ˚C) with initial Ir /Ni molar ratios of 1:0, 2:1, 1:1, 1:2 are denoted as Ir/C-NH_3-500, Ir_2Ni/C-NH_3-500, IrNi/C-NH_3-500, $IrNi_2$/C-NH_3-500. The samples (Ir/Ni=1/1, adjusted pH with $NH_3•H_2O$) annealed at 300, 400, 500 and 600 ˚C are denoted as IrNi/C-NH_3-300, IrNi/C-NH_3-400, IrNi/C-NH_3-500, IrNi/C-NH_3-600, respectively.

Instrumental characterization of the catalysts

The morphology of catalyst particles was observed by using transmission electron microscopy (TEM) analyses, with a JEM 2010 EX microscope, operating at 200 kV. An electron microscope with EDX (FEI, model Quanta 200) was used to observe the composition of the catalysts. The electronic structures and surface compositions of the IrNi/C were performed on an ESCLAB MKII (VG Co., United Kingdom). The crystalline phase X-ray diffraction (XRD) patterns were collected on a Philips PW 3040/60 powder diffractometer using Cu Ka source at 30 keV at a scan rate of 4° min^{-1} over the 2θ range of 20°-90°. The microstructural parameters of samples were determined using JADE5 software.

Electrochemical measurements in a three-electrode cell

Electrochemical experiments were conducted in 0.1 M $HClO_4$ at room temperature with a rotating disk electrode (RDE) using a Solartron electrochemistry station. An Ag/AgCl (saturated KCl) and a Pt wire were used as reference and counter electrodes, respectively. All potentials in this study, however, are given relative to the reversible hydrogen electrode (RHE). The working electrode was prepared as follows. 0.5 mg 40 wt% JM Pt/C (conventional Pt/C catalyst from Johnson-Matthey Co. UK) or 1 mg 20 wt% IrNi/C catalyst was dispersed in 800 uL ethanol with 10 uL Nafion solution (0.1 wt% in isopropyl alcohol) and ultrasonicated to form a uniform catalyst ink. Subsequently, a total of 5 uL well-dispersed catalyst ink was applied onto the prepolished RDE. After drying at room temperature, a drop of 0.01 wt% Nafion solution was applied onto the surface of the catalyst layer to form a thin protective film. The apparent surface area of the glassy carbon disk is 0.19625 cm^2, thus, for all electrochemical experiments on RDE, the specific loadings of Pt and IrNi were equivalent, i.e., 6.37 ug Pt cm^{-2} and 6.37 ug IrNi cm^{-2}. Cyclic voltammograms (CVs) for the catalysts were obtained in a N_2-purged 0.1 M $HClO_4$ from 0.05 to 1.15 V versus RHE at 50 mV s^{-1}. After the CVs did not change, the polarization curve for the HOR was recorded in H_2-saturated 0.1 M $HClO_4$ by sweeping the potential from 0.0 to 0.4 V versus RHE at a scan rate of 10 mV s^{-1} and rotation rate of 1600 rpm.

MEA fabrication and Single cell performance measurements

The membrane electrode assembly (MEA) was fabricated by the following strategies. (i) For non-platinum anode, the catalyst ink was prepared by mixing 20 wt% IrNi/C-NH_3-500 with a solution of 5 wt% Nafion (Dupont) and isopropanol. The weight ratio of IrNi/C catalysts to Nafion was 3:1. The catalyst ink was then sprayed onto the carbon fiber paper giving a loading of 0.2 mg

IrNi cm^{-2}, followed by drying in a vacuum oven at 50 ˚C for 1h. (ii) For standard platinum cathode, the catalyst ink was prepared by mixing 40 wt% JM Pt/C with a solution of 5 wt% Nafion (Dupont) and isopropanol. The weight ratio of JM Pt/C to Nafion was 3:1. The catalyst loading on the carbon fiber paper was 0.3 mg Pt cm^{-2}. The MEA was fabricated by sandwiching the Nafion 212 membrane between the anode and cathode by hot pressing at 135 ˚C and 50 kg cm^{-2} for 150 s. The geometric area of the electrodes is 5 cm^2. The single-cell PEMFC performance was carried out at 80 ˚C and 0.1 MPa with pure hydrogen and oxygen as gas reactants. The flux of H_2 and O_2 was fixed at 200 ml min^{-1} and 300 ml min^{-1}, respectively.

Results and discussions

Physical characterization

Fig. 2 shows representative TEM images of IrNi/C-NH_3-500, which exhibited the best HOR catalytic activity among all the IrNi/C samples discussed later. Uniform sized and spherical shaped IrNi NPs on the carbon support are shown clearly in Fig. S1†. The histogram based on the statics of more than 150 particles in Fig. 2 reveals the narrow size distribution between 1.2 and 3.3 nm and an average particle size of 2.1 nm of the NPs.

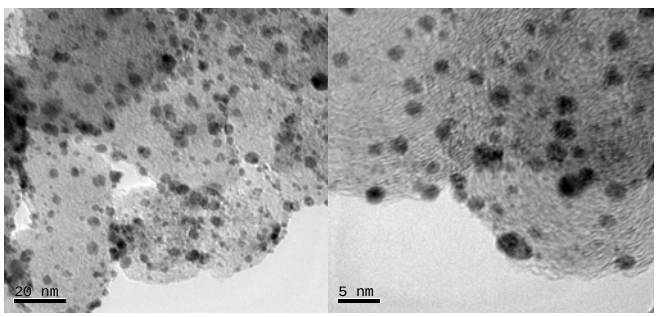

Fig. 2 TEM images of IrNi/C -NH_3-500.

Element	Weight %	Atomic %
C	90.4	97.3
N	0.1	0.1
O	2.4	2
Ir	6	0.4
Ni	1	0.2
Total	100	100

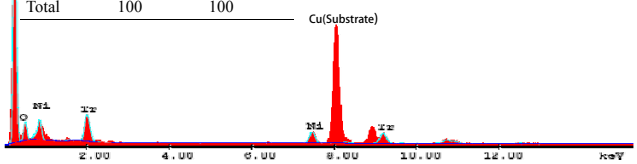

Fig. 3 EDS image and composition data of IrNi/C-NH_3-500.

The final composition of the IrNi/C-NH_3-500 is given by the energy-disperse X-ray spectra (EDS) (Fig. 3). It indicates an atomic ratio of Ir/Ni ≈ 2/1, larger than the initial molar ratio of 1/1, suggesting the partial loss of Ni in the preparing procedure, more likely in the evaporation stage. Besides, a little amount of N coming from ammonia is incorporated in the catalysts with a bulk content of 0.1 at%. It's noteworthy that there is no chloride or other residue detected by EDS, indicating a complete removal of the detrimental species by the facile preparing and washing procedure. The X-ray photoelectron spectroscopy (XPS) (Fig. S2†) of the catalysts confirmed the partial loss of Ni and incorporation of N into the carbon support. Additionally, the XPS also indicates that Ir is present mostly in a metallic state, while both Ni^0 and oxidized Ni are existed because partial Ni is surface-oxidized by long time ambient exposure.

Catalytic activity toward HOR

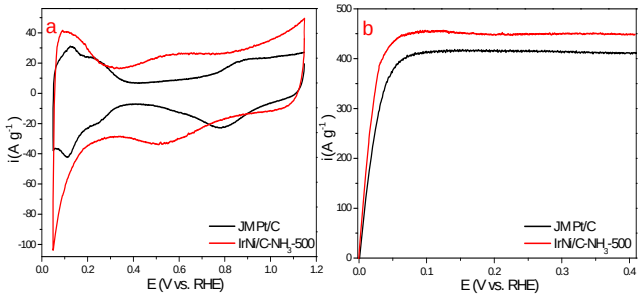

Fig. 4 (a) CV curves for the IrNi/C-NH_3-500 and JM Pt/C catalysts in a de-aerated 0.1 M $HClO_4$ solution (Sweep rate: 50 mV s^{-1}); (b) Polarization curves of H_2 oxidation for IrNi/C-NH_3-500 and JM Pt/C catalysts in a H_2-saturated 0.1 M $HClO_4$ solution at 1600 rpm (Sweep rate: 10 mV s^{-1}). The theoretic catalyst loadings are 6.57 ug Pt cm^{-2}, 6.57 ug IrNi cm^{-2}, respectively.

Fig. 4a shows the CV curves for the IrNi/C-NH_3-500 and the commercial JM Pt/C catalyst in a de-aerated 0.1 M $HClO_4$ solution. Based on the CV curves, the electrochemical surface areas (ECSAs) of the catalysts were measured by the charge collected in the H_{upd} adsorption/desorption region, assuming the hydrogen charge density to be 220 and 210 μC cm^{-2} for Ir and Pt, respectively.[16] The calculation results show that the specific ECSAs (the ECSA per unit weight of Ir and Pt) are 76.7 m^2 g_{IrNi}^{-1} and 63.6 m^2 g_{Pt}^{-1}, respectively. The larger specific ECSA of IrNi/C-NH_3-500 can be attributed to solid/electrolyte interface increase caused by the presence of Ni in IrNi. Fig. 4b gives the polarization curves of HOR on IrNi/C-NH_3-500 and JM Pt/C. The behavior of IrNi/C-NH_3-500 catalyst appears very similar to that observed on Pt, which is known as the best electrocatalyst for H_2 oxidation. The current exhibits rapid rise from zero to diffusion-limited plateau within less than 100 mV. A high limit current density of 458 A g_{IrNi}^{-1} at 0.1 V vs RHE is given by IrNi/C-NH_3-500, which is even 11% higher than that of JM Pt/C (411 A g_{Pt}^{-1}).

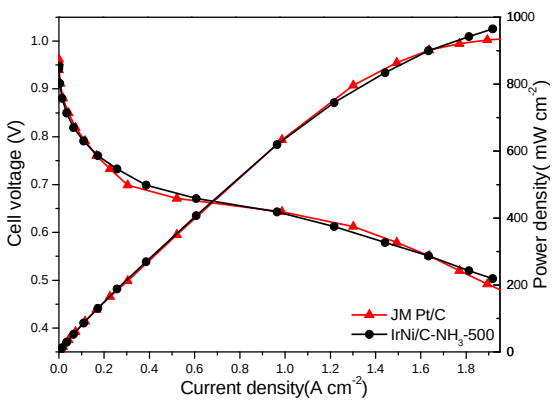

Fig.5 Performance of the MEA with an IrNi/C-NH_3-500 anode (0.2 mg IrNi cm^{-2}) and JM Pt/C cathode (0.3 mg Pt cm^{-2}) cathode , and MEA with JM Pt/C anode (0.2 mg Pt cm^{-2}) and JM Pt/C cathode (0.3 mg Pt cm^{-2}) at 80 ˚C and 0.1

MPa at anode and cathode. H_2 and O_2 were fed at a rate of 200 and 300 ml min^{-1}, respectively.

Fig. 5 shows the current-voltage curve for a single PEMFC with the IrNi/C-NH_3-500 anode (0.2 mg IrNi cm^{-2}) and JM Pt/C cathode (0.3 mg Pt cm^{-2}). For a comparison, the polarization curve of a MEA with conventional JM Pt/C anode (0.2 mg Pt cm^{-2}) and JM Pt/C cathode (0.3 mg Pt cm^{-2}) is also shown in Fig. 5. The open-circuit potentials are both kept at a high level of about 0.97 V. Furthermore, the maximum power density of the MEA with the non-Pt anode is as high as 960 mW cm^{-2}, which is as good as that of the conventional JM Pt/C MEA. The result strongly indicates that the invented IrNi/C catalyst is a promising substitute of commercial Pt/C catalysts in PEMFC anode with much lower cost and comparable performance.

Discussion

It's well known that HOR on a fuel cell anode catalyst is a structure sensitive reaction as represented by the different HOR activity related to the change in size, shape, and structure of NPs [24-26]. Therefore, from the first principle of bimetallic catalysts design[27], accurate control over nucleation and growth stages is of great importance to achieve IrNi bimetallic nanocrystals with well-defined composition, size and microstructure. Herein, by varying thermodynamic and kinetic parameter such as pH regulator, annealing temperature and molar ratio of metal precursor, much effort has been done to optimize the catalytic activity and elucidate the mechanism of this novel synthesis procedure.

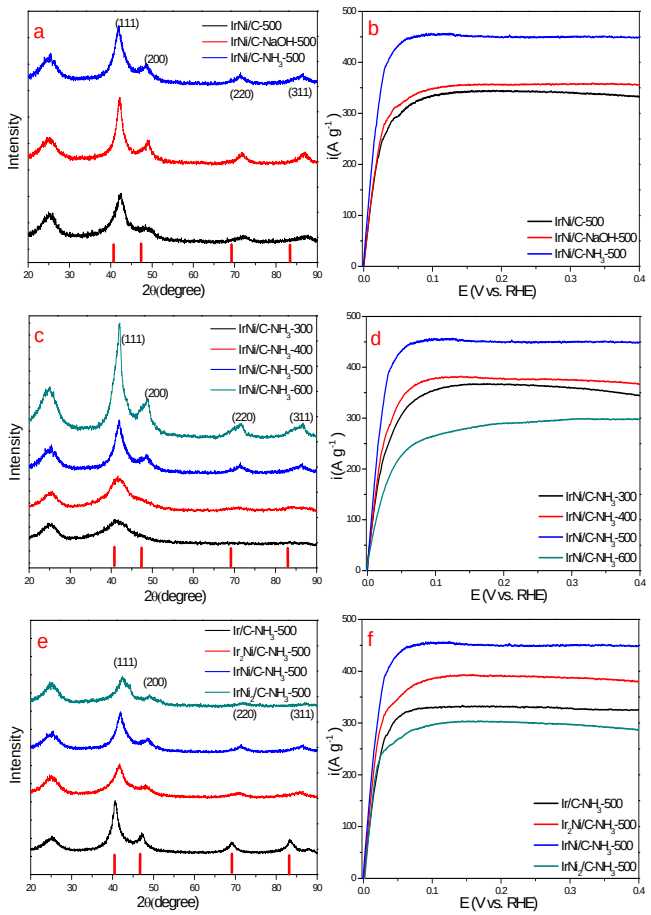

Fig. 6 XRD patterns and corresponding polarization curves of HOR in a H_2-saturated 0.1 M $HClO_4$ solution at 1600 rpm (Sweep rate: 10 mV s^{-1}) for all IrNi/C samples. The theoretic catalyst loadings in HOR tests are 6.57 ug IrNi cm^{-2} for all IrNi/C samples. (a) and (b): samples synthesized at different pH regulator. (c) and (d): samples synthesized at different annealing temperatures. (e) and (f): samples synthesized at different initial Ir/Ni molar ratios.

Fig. 6a shows the XRD patterns of the IrNi/C catalysts synthesized at different pH regulator. For IrNi/C-500 catalyst, which was synthesized without PH adjusting, the ambiguous 200, 211, 311 planes indicate the poor crystallinity. Although IrNi/C-NaOH-500 and IrNi/C-NH_3-500 both have fcc structures, the mean size of IrNi/C-NaOH-500 NPs estimated from the XRD pattern is much larger than those of the other two samples (listed in Table S1†). This difference suggests that the ammonia plays a key role in the catalyst size and microstructure during the nucleation and growth process of the NPs. Fig. 6b reveals that IrNi/C-NH_3-500 gives a much higher mass activity than IrNi/C-500 and IrNi/C-NaOH-500. Coinciding with the XRD analysis, the result confirms that ammonia does have a great impact on the activity of the catalysts.

Fig. 6c and 6d give the XRD patterns and polarization curves of H_2 oxidation of IrNi/C catalysts synthesized at different annealing temperatures. As expected, both the intensity and sharpness of the Ir (111) diffraction peak gradually increases with annealing temperature due to the bigger particle size, stronger contraction of the lattice and larger degree of alloying between Ir and Ni. The absence of 200, 211, 311 diffraction peaks of catalysts synthesized at 300 and 400 ˚C indicates the disordered fcc structure of the NPs. While the heat-treatment at 600 ˚C leads to a sharp increase of the NPs size, indicating sinter of the NPs. Fig. 6d reveals that the HOR activity increases with increasing annealing temperature and reaches a maximum when the heat-treatment temperature is 500˚C. However, the HOR activity of IrNi/C-NH_3-600 drops sharply for the sinter of the NPs, which is fairly in line with the XRD analysis.

Fig. 6e and 6f give the XRD patterns and polarization curves of H_2 oxidation of IrNi/C catalysts synthesized at different initial Ir/Ni molar ratios. Obviously, as the content of Ni increases, the diffraction peaks shift to a higher angle, indicating stronger contraction of the lattice as a consequence of Ni diffusing into the Ir cluster. Moreover, due to the grain refinement and strain effect of bimetallic NPs, the average particle sizes of all IrNi/C samples are sub-3 nm, much smaller than that of Ir/C sample. Fig. 6f reveals that the initial molar ratio of metal precursors has great influence on the catalytic activity and the optimal initial molar ratio of Ir/Ni is 1/1.

The mass activity and corresponding structural parameters including the Ir (111) peak position, d-spacing, lattice parameter and average particle size calculated from Scherrer's equation are all listed in Table S1†. Interestingly, a volcano-shaped correlation is obtained when the measured mass activity is plotted against the corresponding lattice parameter of Ir, with IrNi/C-NH_3-500 which has a lattice parameter of 3.7325 Å occupying the apex of the volcano, as shown in Fig. 7. Coincidently, a classical volcano-shaped correlation between the HOR activity and the hydrogen adsorption free energies has already been found[28-31], with metals that adsorb H_2 neither strongly nor weakly (the Pt group metals) occupying the apex of

the volcano curve. For the first time, we report the volcano-shaped dependence between the HOR mass activity and the lattice parameter of catalysts from electrochemical tests. Obviously, the geometrical effect, i.e. contraction in Ir-Ir bond with Ni introduction, pH adjustor and annealing temperature plays a predominant influence on the adsorption of reactants (H_2) and desorption of intermediates (H_{ad}). We conclude that the optimal Ir-Ir bond distance obtained by controlling the synthesis conditions leads to the optimal interaction between the catalyst surface and the hydrogen intermediates (Ir-H_{ad}), and consequently increases the HOR activity. The high specific ECSA due to the appropriate size and good dispersion of the as synthesized NPs is also an important reason for the excellent HOR catalytic activity.

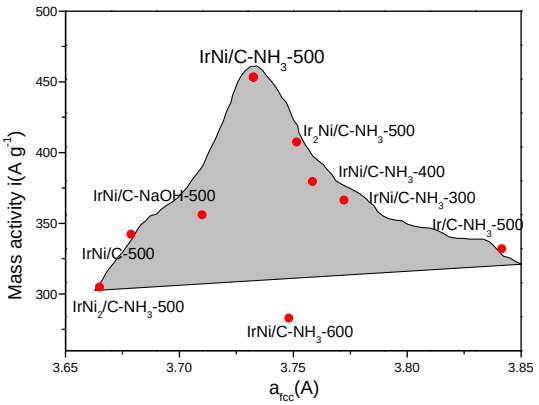

Fig. 7 The volcano-shaped correlation. The data points are the mass activity plotted versus the calculated a_{fcc} of Ir from the XRD patterns. The data points fall on a volcano-shaped curve as expected, with only IrNi/C-NH_3-600 as an exception due to its large size caused by sinter of NPs.

Conclusions

In summary, we have first presented a facile SE-HR strategy to synthesize IrNi/C catalysts with high HOR activity in PEMFCs. The size and the crystal structure of the NPs can be modified by simply varying the preparation conditions, hence to optimize the HOR activity. The catalytic activity of IrNi/C showed the volcano-shaped dependence on the lattice parameter of Ir, and the highest activity was obtained at approximately 3.7325 Å. It's proposed that the enhanced electrocatalytic activity is a result of the optimal interaction between the catalyst surface and hydrogen intermediates, good dispersion of IrNi NPs, and possible synergetic co-catalytic effect of Ir and Ni. This novel SE-HR strategy seems especially efficient for tailoring the properties of IrNi NPs as one of the promising Pt-alternative catalysts.

Acknowledgements

This work was financially supported by China National 973 Program (2012CB215500 and 2012CB720300), by NSFC of China (Grant Nos. 21276291 and 21176327) and by the Fundamental Research Funds for the Central Universities (CDJZR12228802).

Notes and references

The State Key Laboratory of Power Transmission Equipment & System Security and New Technology, College of Chemistry and Chemical Engineering, Chongqing University, Chongqing, 400044, P. R. China. Fax: 86 6510; Tel: 86 6510; E-mail: zdwei@cqu.edu.cn.

† Electronic Supplementary Information (ESI) available: [details of any supplementary information available should be included here]. See DOI: 10.1039/b000000x/

1 B. C. H. Steele and A. Heinzel, *Nature*, 2001, **414**, 345–352.
2 J. Xie, D. L. Wood, K. L. More, P. Atanassov and R. L. Borup, *J. Electrochem. Soc.*, 2005, **152**, A1011–A1020.
3 T. J. Schmidt, V. Stamenkovic, N. M. Markovic and P. N. Ross, *Electrochim. Acta*, 2003, **48**, 3823–3828.
4 Y. P. Xiao, W. J. Jiang, S. Wan, X. Zhang, J. S. Hu, Z. D. Wei and L. J. Wan, *Journal J. Mater. Chem. A*, 2013, **1**, 7463-7468. 4.
5 D. J. Ham, C. Pak, G. H. Bae, S. Han, K. Kwon, S. A. Jin, H. Chang, S. H. Choic, and J. S. Lee, *Chem. Commun.,* 2011, **47**, 5792–5794.
6 J. Snyder, T. Fujita, M. W. Chen and J. Erlebacher, *Nat. Mater.*, 2010, **9**, 904–907.
7 R. Bashyam and P. Zelenay, *Nature*, 2006, **443**, 63-66.
8 W. Ding, Z. Wei, S. Chen, X. Qi, T. Yang, J. Hu, D. Wang, L. J. Wan, S. F. Alvi and L. Li, *Angewandte Chemie*, 2013, **125**, 11971–11975.
9 M. Xia, W. Ding, K. Xiong, L. Li, X. Qi, S. Chen, B. Hu and Z. Wei, *J. Phys. Chem. C*, 2013, **117**, 10581–10588.
10 H. Yin, C. Zhang, F. Liu and Y. Hou, *Adv. Funct. Mater.*, 2014, doi: 10.1002/adfm.201303902.
11 H. A. Gasteiger, J. E. Panels and S. G. Yan, *J. Power Sources*, 2004, **127**, 162.
12 D. J. Ham and J. S. Lee, *Energies*, 2009, **2**, 873.
13 D. A. J. Rand and R. Woods, *J. Electroanal. Chem.*, 1974, **55**, 375–381.
14 Platinum today, http://www.platinum.matthey.com/publications/price-reports.html.
15 B. Li, J. L. Qiao, J. S. Zheng, D. J. Yang and J. X. Ma, *J. Hydrogen Energy*, 2009, **34**, 5144–5151.
16 B. Li, J. L. Qiao, D. J. Yang, R. Lin, H. Lv, H. J. Wang and J. X. Ma, *Int. J. Hydrogen Energy*, 2010, **35**, 5528–5538.
17 D. J. Yang, B. Li, H. Zhang and J. X. Ma, *Fuel Cells*, 2013, **13**, 309–313.
18 K. Sasaki, K. Kuttiyiel, L. Barrio, D. Su, A. I. Frenkel, N. Marinkovic, D. Mahajan and R. Adzic, *J. Phys. Chem. C*, 2011, **115**, 9894–9902.
19 M. Haruta, *Catal. Today*, 1997, **36**, 153–166.
20 K. Shimizu, K. Sugino, K. Sawabe, A. Satsuma, *Chem. Eur. J.,* 2009, **15**, 2341–2351.
21 C. Yang, H. Zhao, Y. Hou and D. Ma, *J. Am. Chem. Soc.*, 2012, **134**, 15814–15821.
22 P. Rodriguez, F. D. Tichelaar, M. T. M. Koper and A. I. Yanson, *J. Am. Chem. Soc.*, 2011, **133**, 17626–17629.
23 H. Chen, D. L. Wang, Y. C. Yu, K. A. Newton, D. A. Muller, H. Abruña and F. J. DiSalvo, *J. Am. Chem. Soc.*, 2012, **134,** 18453–18459.
24 J. Ohyama, T. Sato, Y. Yamamoto, S. Arai and A. Satsuma, *J. Am. Chem. Soc.*, 2013, **135**, 8016–8021.
25 B. E. Conway and B. V. Tilak, *Electrochim. Acta*, 2002, **47**, 3571–3594.
26 D. Strmcnik, M. Uchimura, C. Wang, R. Subbaraman, N. Danilovic, D. Vliet, A. P. Paulikas, V.R. Stamenkovic and N. M. Markovic. *Nat. Chem.*, 2013, **5**, 300–306.
27 J.Greeley and M. Mavrikakis, *Nat. Mater.*, 2004, **3**, 810–815.
28 J. K. Norskov, T. Bligaard, J. Rossmeisl and C. H. Christensen. *Nat. Chem.*, 2009, **1**, 37–46.
29 E. Santos, P. Hindelang, P. Quaino, E. N. Schulz and G. Soldano, *ChemPhysChem*, 2011, **12**, 2274–2279.
30 Y. C. Weng and C. T. Hsieh, *Electrochim, Acta*, 2011, **56**, 1932–1940.
31 E. Skúlason, V. Tripkovic, M. E. Björketun, S. Gudmundsdóttir, G. Karlberg, J. Rossmeisl, T. Bligaard, H. Jónsson and J. K. Nørskov, *J. Phys. Chem. C*, 2010, **114**, 18182–18197.